Toward ultrahigh thermal conductivity graphene films

Toward ultrahigh thermal conductivity graphene films

2D Materials

PAPER

Toward ultrahigh thermal conductivity graphene films

Sihua Guo[1,7], Shujin Chen[1,7], Amos Nkansah[2,7], Abdelhafid Zehri[3,7], Murali Murugesan[2], Yong Zhang[1,*], Yan Zhang[1], Chen Yu[1], Yifeng Fu[3], Markus Enmark[3], Jin Chen[4], Xinfeng Wu[5], Wei Yu[6] and Johan Liu[1,3,6,*]

[1] SMIT Center, School of Mechatronics Engineering and Automation, Shanghai University, 20 Chengzhong Rd., Shanghai 201800, People's Republic of China
[2] SHT Smart High-Tech AB, Kemivägen 6, Se 412 58, Gothenburg, Sweden
[3] Electronics Materials and Systems Laboratory, Department of Microtechnology and Nanoscience, Chalmers University of Technology, Kemivägen 9, Se 412 96, Gothenburg, Sweden
[4] Shanghai Ruixi New Materials High-Tech Ltd, Fengxian District, Shanghai, People's Republic of China
[5] Shanghai Marina University, Shanghai, People's Republic of China
[6] Shanghai Polytech University, Shanghai, People's Republic of China
[7] Equal contributor.
[*] Authors to whom any correspondence should be addressed.

E-mail: yongz@shu.edu.cn, jyliu@sspu.edu.cn and jliu@chalmers.se

Keywords: graphene assembled film, ultrahigh thermal conductivity, heat treatment time

Supplementary material for this article is available online

OPEN ACCESS

RECEIVED
8 September 2022

ACCEPTED FOR PUBLICATION
22 September 2022

PUBLISHED
12 October 2022

Abstract

With increasing demands of high-performance and functionality, electronics devices generate a great amount of heat. Thus, efficient heat dissipation is crucially needed. Owing to its extremely good thermal conductivity, graphene is an interesting candidate for this purpose. In this paper, a two-step temperature-annealing process to fabricate ultrahigh thermal conductive graphene assembled films (GFs) is proposed. The thermal conductivity of the obtained GFs was as high as 3826 ± 47 W m^{-1} K^{-1}. Extending the time of high-temperature annealing significantly improved the thermal performance of the GF. Structural analyses confirmed that the high thermal conductivity is caused by the large grain size, defect-free stacking, and high flatness, which are beneficial for phonon transmission in the carbon lattice. The turbostratic stacking degree decreased with increasing heat treatment time. However, the increase in the grain size after long heat treatment had a more pronounced effect on the phonon transfer of the GF than that of turbostratic stacking. The developed GFs show great potential for efficient thermal management in electronics devices.

1. Introduction

With the rapid development of high-performance electronics, heat dissipation has become a critical issue that restricts their development, and the demand for heat dissipation in electronics devices has rapidly increased [1–3]. An effective strategy to solve this problem is to integrate high-thermal-conductivity materials at hot spots to reduce the temperatures of the heat sources [4]. Traditional heat-dissipation materials are metal materials or artificial graphite films, but it is difficult for these materials to meet the heat-dissipation requirements of high-power electronics devices [5].

Graphene is two-dimensional single-layer graphite, and it has received extensive attention in thermal management owing to its extraordinary thermal conductivity and mechanical properties [6, 7]. Graphene oxide (GO) sheets can be easily assembled into a thin film with a layered structure through a solution process [8], and GO is generally used as the precursor to prepare graphene assembled films (GFs) [9]. Various methods for preparing GO films have been developed, including vacuum filtration, spin coating, rod coating, evaporation-assisted self-assembly, and electro-induced deposition [10–14]. The oxygen groups in GO sheets destroy the conjugated sp^2 network of graphene, resulting in a significant decrease in the thermal conductivity [15]. Methods to repair the structural defects of GO films include ascorbic acid reduction, hydrazine reduction, and other chemical reductions [16–18]. However, the remaining

defective structures after chemical reduction can still hinder phonon transmission in the carbon lattice. Many researchers have reported preparation of GFs by high-temperature annealing of GO. The effective removal of the oxygen-containing groups and repair of the sp^2 structure in graphene during the high-temperature annealing process can effectively improve the thermal conductivity of GFs [19]. Chen *et al* [20] reported GFs with thermal conductivity of 1204 W m^{-1} K^{-1} fabricated by thermal annealing at 1500 °C and 2850 °C. Peng *et al* [21] prepared GFs with thermal conductivity of 1940 W m^{-1} K^{-1} by extremely high temperature annealing at 3000 °C. Zhang *et al* [22] reported GFs with thermal conductivity of up to 1224 W m^{-1} K^{-1} fabricated by thermal annealing at 2800 °C. Clearly, improving the thermal conductivity of GFs is an interesting topic that has attracted the attention of many researchers.

In this paper, we report the effect of the heat treatment time for reduced self-assembly of GO film at 2850 °C on the thermal conductivity. The thermal conductivity of the obtained GFs reached a remarkable value of 3826 ± 47 W m^{-1} K^{-1}. The significant enhancement of the thermal conductivity can be attributed to the large grain size, defect-free stacking, and high flatness of the GF. Molecular dynamics (MDs) simulation showed that the turbostratic lattice can improve the in-plane thermal conductivity of the GF, but the turbostratic degree decreased with increasing heat treatment time. However, the increase in the thermal conductivity due to the increase in the grain size outweighed the decrease in the thermal conductivity due to the decrease in the turbostratic degree.

2. Experimental section

2.1. Materials

Expanded graphite was obtained from the Superior Graphite Company, Germany. Concentrated sulfuric acid (98%), potassium permanganate, sodium nitrate, and hydrogen peroxide aqueous solution (30%) were obtained from Sigma-Aldrich. All of the reagents were analytical grade.

2.1.1. Preparation of GO

GO was synthesized by the modified Hummer's method, similar to previous reports [7, 23]. In brief, expanded graphite (5 g) was placed in concentrated H_2SO_4 (200 ml) and $NaNO_3$ (3.75 g) while stirring in an ice bath. Subsequently, $KMnO_4$ (15 g) was gradually added for 1 h with stirring, and the temperature of the mixture was maintained at the freezing point. The mixture was then heated to 32 °C–40 °C, and stirring was continued for 1 h. Next, 5 wt% H_2SO_4 (400 ml) was added to the mixture, and the mixture was heated at 98 °C for 1 h. The temperature of the mixture was then lowered to 60 °C, and 30% H_2O_2 (15 ml) was added to the mixture with slow stirring. The product was centrifuged and washed with deionized water until the pH value was close to 7. The obtained colloid was dispersed in deionized water to obtain a certain concentration of GO solution. GO was stripped by high-speed shear mixing for 1 h. After shear mixing, the obtained GO suspension was centrifuged at 9000 rpm for 30 min to remove all of the large particles and thicker GO sheets, thereby obtaining a uniform GO solution.

2.1.2. Preparation of the GFs

The GFs were fabricated by the process described in figure 1, including self-assembly, two-step graphitization, and mechanical pressing. Formation of the GFs occurred by random stacking and self-assembly of GO sheets. The graphitization process of the reduced GO (RGO) film can be divided into two steps. In the first step, the oxygen-containing functional groups were removed and atomic vacancies were generated in the RGO film at 1500 °C. In the second step, annihilation of the atomic vacancies occurred and the overlapping sheets on RGO combined to form a continuous polycrystalline layer at 2850 °C. Finally, a high-density GF film was obtained after 300 MPa mechanical compression. To obtain differently graphitized GFs, the GFs were graphitized at 2850 °C for 1, 2, 3, and 4 h, and the GFs are denoted as GF-1, GF-2, GF-3, and GF-4, respectively.

2.2. Characterization

X-ray diffraction (XRD), x-ray photoelectron spectroscopy (XPS), and Raman spectroscopy were performed to determine the oxygen and defect contents of the GFs. The surface morphology of the GFs was investigated by scanning electron microscopy (SEM), and the cross-section morphology was observed by SEM with a focused ion beam (FIB). The lattice images of the GFs were obtained by transmission electron microscopy (TEM). The surface roughness of the GFs was characterized by atomic force microscopy (AFM). The in-plane thermal conductivity of the GFs was evaluated by Joule self-heating method.

3. Results and discussion

The essence of heat conduction in graphene is phonon transport in the sp^2 carbon lattice [24–26]. Thus, high crystallinity and large grain size are essential to improve the thermal conductivity of GFs. In this study, the GFs were annealed at a high temperature of 2850 °C to eliminate most of the defects and form a graphene layer with continuous orientation. The structure restoration of the GFs during heat treatment was characterized by XPS, XRD, and Raman spectroscopy. With extension of the annealing time at 2850 °C from 1 to 4 h, the ratio of carbon to oxygen atoms increased from 17 to 47, while the O 1s peak

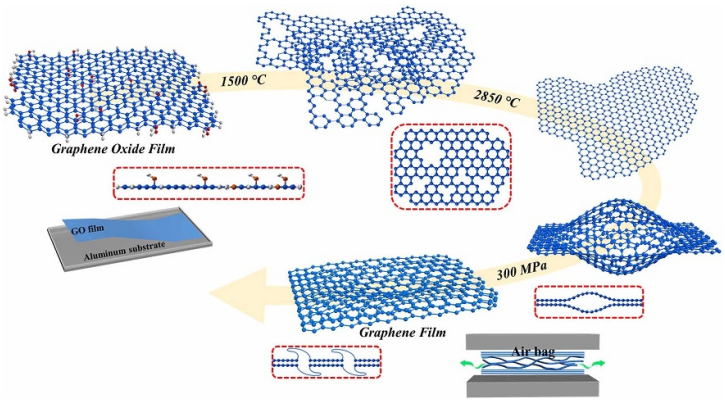

Figure 1. Schematic illustration of the GF fabrication process.

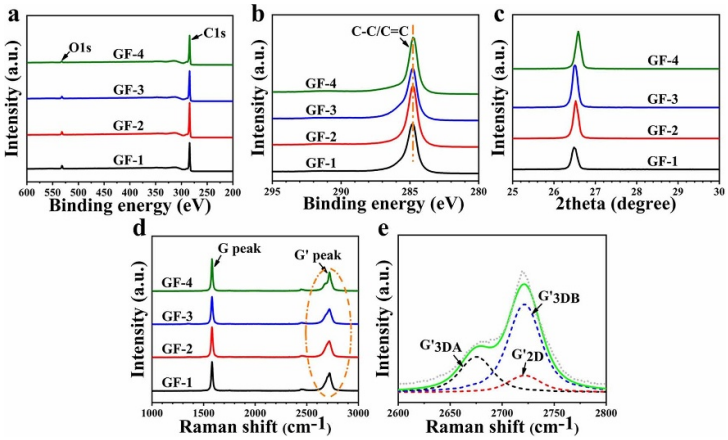

Figure 2. (a) XPS spectra showing the elemental compositions, (b) high-resolution C 1s spectra, (c) XRD spectra of crystallinity evolution and interlaminar consolidation, and (d) Raman spectra of GF-1, GF-2, GF-3, and GF-4. (e) Lorentzian fitting of the measured Raman G′ peak of GF-4.

almost disappeared, as shown in figure 2(a). In addition, the C–C/C=C peak became sharp and obvious after graphitization (figure 2(b)), indicating that the sp^2 lattice of the GF was significantly repaired by the 2850 °C high-temperature annealing process, which agrees well with previous studies [4, 27].

The GFs showed a sharp diffraction peak at approximately 26.5° in the XRD spectra (figure 2(c)), indicating that the GFs were highly crystalline after graphitization [28]. By increasing the annealing time at 2850 °C, the *d* spacing of the GF decreased from 0.337 nm for GF-1 to 0.335 nm for GF-4, which is close to the *d* value of 0.3355 nm for highly oriented graphite [19]. The decrease of the interlayer spacing is attributed to effective removal of the oxygen-containing groups on the basal plane of the GFs. According to Scherrer's equation [29], the in-plane grain size (L_c) of GF-4 was estimated to be 59 nm, which was significantly larger than that of GF-1 (50 nm). Both the grain size and grain boundaries affect the thermal properties of GFs. Grain boundaries cannot be annihilated by high-temperature graphitization [30], but an increase of the grain size can effectively reduce the number of grain boundaries. The large grain size of GF-4 can greatly reduce phonon defects and boundary scattering, thereby significantly improving phonon transmission in the GF.

Raman spectroscopy was performed to investigate defect repair of the GFs during heat treatment. The D peak of the GFs disappeared, as shown in figure 2(d), indicating that the structural defects of the GFs were effectively repaired by annealing at 2850 °C [31, 32]. The G′ peak is sensitive to the presence of structural disorder. Linear analysis of the G′ peak can reveal the three-dimensional stacking structure inside the sample. Lorentzian fitting of the measured Raman G′ peak of GF-4, consisting of turbostratic stacking (G′2D) and AB Bernal stacking (G′3DA, G′3DB), is shown in figure 2(e). Based on Cancado's equation [33], the relative percentages of turbostratic stacking for GF-1, GF-2, GF-3, and GF-4 were calculated to be 34%, 35%, 33%, and 23%, respectively (figure S1).

We believe that turbostratic stacking has several forms, including rotation and intersection between the sheets. MD simulation was performed to investigate the influence of the presence of turbostratic

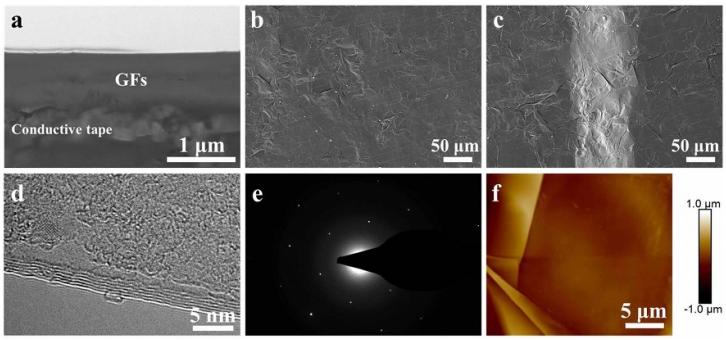

Figure 3. (a) Cross-sectional FIB-SEM image of GFs. (b) Top view of the surface of GFs. (c) Top view of the surface of GFs after 5000 bending/release cycles. (d) High-resolution TEM image of the edge morphology of GFs. Electron diffraction pattern of the GF in (e), (f) AFM image showing the morphology of GF-4.

stacking on the heat transfer of the GF in the out-of-plane and in-plane directions (figure S2). The heat transfer was closely related to the stacking pattern. A previous study has shown that turbostratic stacking can lead to lower interlayer binding energy, enhancing heat transfer in the plane [4]. A similar result was obtained in this study.

The percentage of turbostratic stacking in the GF decreased with increasing high-temperature annealing time, decreasing the in-plane thermal conductivity. Ma *et al* [34] reported that the grain size has a significant effect on the thermoelectric properties of graphene. In summary, the effect of the increase of the grain size with increasing heat treatment time was greater than the effect of the decrease of turbostratic stacking. Therefore, the thermal conductivity still increased with increasing heat-treatment time.

Artificial tearing can destroy the original morphology of the sample (figure S4). To obtain a better cross-sectional morphology of the GFs, SEM with a FIB was performed. During the annealing process, gas molecules, such as CO or CO_2, expand in the multilayer graphene sheets and can form micro-airbags [35, 36], which is harmful to the transfer of heat flow. Micro-airbags were found in the GFs before mechanical pressing in this study (figure S3). Interestingly, the GFs showed very high density and defect-free structures with a thickness of approximately 1 μm after mechanical pressing (figure 3(a)). The dense and defect-free stacking structure facilitates phonon transmission, which enhances the thermal conductivity. To demonstrate the flexibility of the obtained GFs, bending tests were performed. After 5000 bending/release cycles, the GFs exhibited good flexibility and reliability without any fracture, as shown in figure 3(c). The stretchable micro-folds make GFs have a wide elastic region, which can restore the original structure under repeated deformation (figure 3(b)) [21]. A high-resolution TEM image of the edge morphology of GF, which was composed of six layers of graphene, is shown in figure 3(b). The well-defined diffraction spots showed that the graphene sheets had an sp^2 crystalline structure (figure 3(e)).

In addition to the large grain size, roughness of the surface of the GF can also cause phonon scattering [4]. Therefore, the flatness of the film surface plays an important role in the thermal conductivity of GFs. With extension of the annealing time at 2850 °C, the overlapping graphene sheets combined to form non-overlapping, extended, and flat graphite layers. The size of the smooth features increased from 8.5 μm for GF-1 to 20 μm for GF-4 (figures 3(f) and S6). A longer high-temperature annealing time eliminated the rough morphology, resulting in enhancement of the thermal conductivity.

The in-plane thermal conductivities of the GFs were measured by a previously reported Joule self-heating method [4]. GF-4 showed the highest in-plane thermal conductivity of 3826 ± 47 W m^{-1} K^{-1}, which was 39% higher than that of GF-1 (figure 4(a)). The GFs showed higher thermal conductivity than previously reported GFs, reduced GFs, and graphite (figure 4(b), for the detailed information, see table S1). At the same time, the electrical conductivity of GFs shows an increasing trend with the extension of heat treatment time (figure S7).

The excellent thermal properties of the GFs can be attributed to the following factors: (a) the improvement of the crystallinity by extending the thermal annealing time at 2850 °C, (b) the dense and defect-free arrangement of the graphene sheets inside the GFs, and (c) the high flatness of the GFs. Extending the annealing time at 2850 °C can effectively repair the defects in the carbon lattice generated by removal of the oxygen-containing groups and improve the flatness of the GF surface, reducing the scattering points of the phonons and leading to significant enhancement of the thermal performance [37–39]. In addition, the dense structure results in high in-plane thermal conductivity.

To further demonstrate the outstanding heat spreading performance of the GFs, we used a self-made thermal test platform to observe the heat

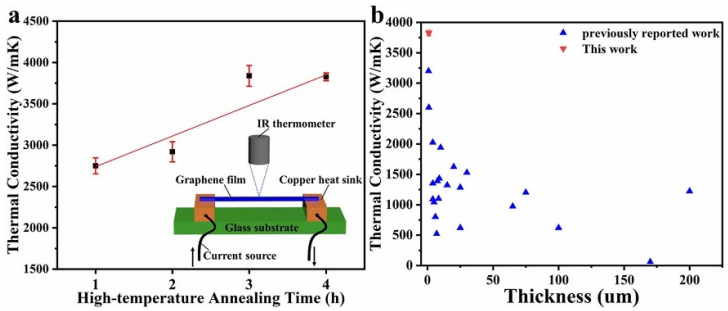

Figure 4. (a) In-plane thermal conductivity of the GFs with different high-temperature annealing time measured by the Joule self-heating method. The insert shows a schematic diagram of the Joule-heating measurement device. (b) Comparison of the thermal conductivity of GFs with previously reported work (for the detailed information, see table S1).

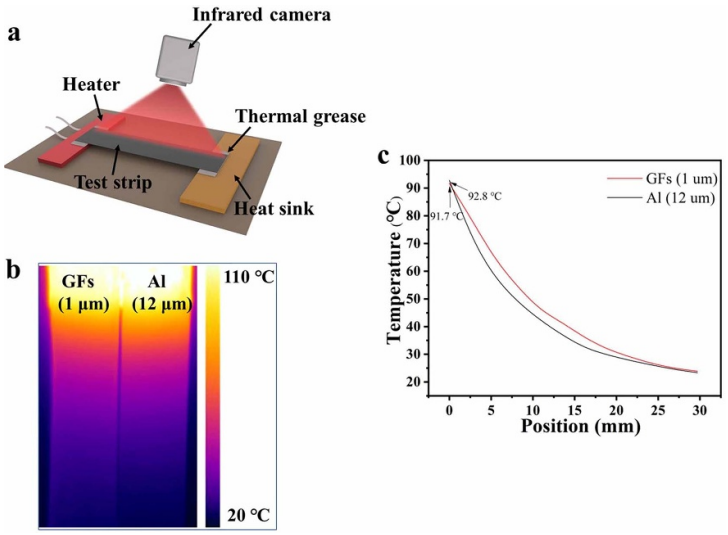

Figure 5. (a) Schematic diagram of the thermal test platform. (b) Infrared image of 1 μm-thick GF and 12 μm-thick aluminum foil. (c) Corresponding temperature curves.

transfer of the GF, as shown in figure 5(a), and we compared the results with that of a 12 μm-thick aluminum foil. Before testing, a thin layer of carbon black was sprayed on the surfaces of the test strips to ensure similar emissivity. Compared with the 12 μm-thick aluminum foil, the 1 μm-thick GF showed a lower temperature gradient, indicating the outstanding heat-transfer capability of the GF (figures 5(b) and (c)). This GF shows potential for rapid heat dissipation in next-generation electronic devices.

For more practical heat dissipation capability demonstration, application tests were performed by loading the GFs on self-made thermal test platform (figure S8(a)). The results show that the high-temperature annealing treatment can effectively increase the heat dissipation capability of the GFs and can be potentially used for thermal management of electronics devices.

4. Conclusions

By extending the high-temperature annealing time, the thermal conductivity of the GF increases. The large grain size (59 nm), highly flat graphene flakes (20 μm), and dense and defect-free structure endow the GF with ultrahigh thermal conductivity of up to 3826 $\pm$ 47 W m^{-1} K^{-1}. We believe that these GFs can be integrated into the next generation of high-performance electronics devices for thermal management.

Data availability statement

All data that support the findings of this study are included within the article (and any supplementary files).

Acknowledgments

Sihua Guo, Yong Zhang, Yan Zhang, Chen Yu and Johan Liu acknowledge the financial support from the National Natural Science Foundation of China (No: 51872182). A Zehri, Y Fu and J Liu also acknowledge the financial support from the Swedish National Science Foundation with the Contract No: 621-2007-4660, Vinnova Siografen as well as from the

Production Area of Advance at Chalmers University of Technology, Sweden. A N and M M acknowledge the financial support from Vinnova Siografen program.

ORCID iDs

Abdelhafid Zehri https://orcid.org/0000-0002-6129-0537
Yong Zhang https://orcid.org/0000-0002-3210-4862
Yan Zhang https://orcid.org/0000-0002-2461-060X
Markus Enmark https://orcid.org/0000-0001-6836-655X
Xinfeng Wu https://orcid.org/0000-0002-8597-8272
Johan Liu https://orcid.org/0000-0001-9931-1439

References

[1] Li H-L, Xiao S-N, Yu H-L, Xue Y-H and Yang J-H 2021 A review of graphene-based films for heat dissipation *New Carbon Mater.* **36** 897–908
[2] Li H, Wu X, Cheng K, Zhu M, Wang L and Yu H 2021 One-pot modified "grafting-welding" preparation of graphene/polyimide carbon films for superior thermal management *New Carbon Mater.* **36** 949–57
[3] Qiu H, Zhao X, Li H, Li Y, Li J and Yang J 2021 Highly flexible and thermal conductive films of graphene/poly(naphthylamine) and applications in thermal management of LED devices *J. Appl. Polym. Sci.* **138** 51383
[4] Wang N, Samani M K, Li H, Chen S and Liu J 2018 Tailoring the thermal and mechanical properties of graphene film by structural engineering *Small* **14** 1801346
[5] Wu T, Xu Y, Wang H, Sun Z and Zou L 2021 Efficient and inexpensive preparation of graphene laminated film with ultrahigh thermal conductivity *Carbon* **171** 639–45
[6] Fu Y, Hansson J, Liu Y, Chen S, Wang N, Zhang Y and Liu J 2019 Graphene related materials for thermal management *2D Mater.* **7** 012001
[7] Zhang Y, Han H, Wan N, Fu Y, Murugesan M, Edwards M and Liu J 2015 Improved heat spreading performance of functionalized graphene in microelectronic device application *Adv. Funct. Mater.* **25** 4430–5
[8] Shen B, Zhai W and Zheng W 2014 Ultrathin flexible graphene film: an excellent thermal conducting material with efficient EMI shielding *Adv. Funct. Mater.* **24** 4542–8
[9] Guo S, Chen J, Zhang Y and Liu J 2021 Graphene-based films: fabrication, interfacial modification, and applications *Nanomaterials* **11** 2539
[10] Dikin D A, Stankovich S, Zimney E J, Piner R D, Nguyen S T and Ruoff R S 2007 Preparation and characterization of graphene oxide paper *Nature* **448** 457–60
[11] Chi C, Wang X, Peng Y, Dong J and Zhao D 2016 Facile preparation of graphene oxide membranes for gas separation *Chem. Mater.* **28** 2921–7
[12] Ma L, Wang Y, Wang Y, Wang C and Gao X 2020 Graphene induced carbonization of polyimide films to prepared flexible carbon films with improving-thermal conductivity *Ceram. Int.* **46** 3332–8
[13] Li H, Dai S, Miao J, Wu X, Qiu H and Yang J 2018 Enhanced thermal conductivity of graphene/polyimide hybrid film via a novel "molecular welding" strategy *Carbon* **126** 319–27
[14] Li J, Zhang P, He H and Shi B 2020 Enhanced the thermal conductivity of flexible copper foil by introducing graphene *Mater. Des.* **187** 108373
[15] Song N-J, Chen C-M, Lu C, Liu Z, Kong Q-Q and Cai R 2014 Thermally reduced graphene oxide films as flexible lateral heat spreaders *J Mater. Chem.* A **2** 16563–8
[16] Guo S, Zheng R, Jiang J, Yu J, Dai K and Yan C 2019 Enhanced thermal conductivity and retained electrical insulation of heat spreader by incorporating alumina-deposited graphene filler in nano-fibrillated cellulose *Composites* B **178** 107489
[17] Gao X, Jang J and Nagase S 2009 Hydrazine and thermal reduction of graphene oxide: reaction mechanisms, product structures, and reaction design *J. Phys. Chem.* C **114** 832–42
[18] Lin Y, Hou G, Bi S, Su X and Li H 2020 Synthesis of reduced graphene oxide paper for EMI shielding by a multi-step process *Funct. Mater. Lett.* **13** 2051024
[19] Rozada R, Paredes J I, Villar-Rodil S, Martínez-Alonso A and Tascón J M D 2013 Towards full repair of defects in reduced graphene oxide films by two-step graphitization *Nano Res.* **6** 216–33
[20] Chen S, Wang Q, Zhang M, Huang R and Liu J 2020 Scalable production of thick graphene film for next generation thermal management application *Carbon* **167** 270–7
[21] Peng L, Xu Z, Liu Z, Guo Y, Li P and Gao C 2017 Ultrahigh thermal conductive yet superflexible graphene films *Adv. Mater.* **29** 1700589
[22] Zhang X, Guo Y, Liu Y, Li Z, Fang W, Peng L and Gao C 2020 Ultrathick and highly thermally conductive graphene films by self-fusion strategy *Carbon* **167** 249–55
[23] Han H, Zhang Y, Wang N, Samani M K, Mijbil Z Y, Edwards M, Murugesan M, Lambert C J, Liu J and Volz S 2016 Functionalization mediates heat transport in graphene nanoflakes *Nat. Commun.* **7** 11281
[24] Nika D L and Balandin A A 2017 Phonons and thermal transport in graphene and graphene-based materials *Rep. Prog. Phys.* **80** 036502
[25] Xu X, Chen J and Li B 2016 Phonon thermal conduction in novel 2D materials *J. Phys. Condens. Matter* **28** 483001
[26] Mu X, Wu X, Zhang T, Go D B and Luo T 2014 Thermal transport in graphene oxide-from ballistic extreme to amorphous limit *Sci. Rep.* **4** 3909
[27] Ganguly A, Sharma S, Papakonstantinou P and Hamilton J W J 2011 Probing the thermal deoxygenation of graphene oxide using high-resolution *in situ* x-ray-based spectroscopies *J. Phys. Chem.* C **115** 17009–19
[28] Chen J, Shi T, Cai T, Xu T, Sun L, Wu X and Yu D 2013 Self healing of defected graphene *Appl. Phys. Lett.* **102** 103107
[29] Cançado L G, Takai K, Enoki T, Endo M, Kim Y A, Mizusaki H, Speziali N L, Jorio A and Pimenta M A 2008 Measuring the degree of stacking order in graphite by Raman spectroscopy *Carbon* **46** 272–5
[30] Kurasch S, Kotakoski J, Lehtinen O, Skakalova V, Smet J, Krill C E, Krasheninnikov A V and Kaiser U 2012 Atom-by-atom observation of grain boundary migration in graphene *Nano Lett.* **12** 3168–73
[31] Zeng Y, Li T, Yao Y, Li T, Hu L and Marconnet A 2019 Thermally conductive reduced graphene oxide thin films for extreme temperature sensors *Adv. Funct. Mater.* **29** 1901388
[32] Ghosh T, Biswas C, Oh J, Arabale G, Hwang T, Luong N D, Jin M, Lee Y H and Nam J-D 2012 Solution-processed graphite membrane from reassembled graphene oxide *Chem. Mater.* **24** 594–9
[33] Malard L M, Pimenta M A, Dresselhaus G and Dresselhaus M S 2009 Raman spectroscopy in graphene *Phys. Rep.* **473** 51–87
[34] Ma T, Liu Z, Wen J, Gao Y, Ren X, Chen H, Jin C, Cheng H-M and Ren W 2017 Tailoring the thermal and electrical transport properties of graphene films by grain size engineering *Nat. Commun.* **8** 14486
[35] Bagri A, Mattevi C, Acik M, Chabal Y J, Chhowalla M and Shenoy V B 2010 Structural evolution during the reduction of chemically derived graphene oxide *Nat. Chem.* **2** 581–7
[36] Fernández P S, Rozada R, Paredes J I, Villar-Rodil S, Fernández-Merino M J, Guardia L, Martínez-Alonso A and Tascón J M D 2012 Chemical and microscopic analysis of

graphene prepared by different reduction degrees of graphene oxide *J. Alloys Compd.* **536** 532–7
[37] Xin G, Sun H, Hu T, Fard H R, Sun X, Koratkar N, Borca-Tasciuc T and Lian J 2014 Large-area freestanding graphene paper for superior thermal management *Adv. Mater.* **26** 4521–6
[38] Song L, Khoerunnisa F, Gao W, Dou W, Hayashi T, Kaneko K, Endo M and Ajayan P M 2013 Effect of high-temperature thermal treatment on the structure and adsorption properties of reduced graphene oxide *Carbon* **52** 608–12
[39] Paredes J I, Fernández P S, Martínez-Alonso A and Tascoń J M D 2009 Atomic vacancy engineering of graphitic surfaces: controlling the generation and harnessing the migration of the single vacancy *J. Phys. Chem.* C **113** 10249–55